IRAS Colors Within M31: Evidence for Deficiency of Very Small Grains?

tong **X u**

Max-Planck-Institut für Kernphysik, Postfach 103980, W6900 Heidelberg, F.R.G.;
Max-Planck-Institut fur Radioastronomie, Auf dem Hügel 69, W5300 Bonn 1, F.R.G.

George Helou

IPAC 100-22, California Institute of Technology, Pasadena, CA 91125

Submitted to The Astrophysical Journal

ABSTRACT

Significant differences are found in the IRAS color-color diagrams of small regions (2' × 2', or 0.4 $kpc \times 1.8\,kpc$) within the disk of M31 compared to Galactic cirrus, most noticeably demonstrated by a trend of low $60\mu m$-to-$100\mu m$ surface brightness ratio and high $12\mu m$-to-$25\mu m$ ratio. Based on physical arguments, we conclude that these color differences are best explained by assuming that "Very Small Grains" (but not Polycyclic Aromatic Hydrocarbons) are only half as abundant in M31 as they are in Galactic cirrus. We confirm this conclusion and test its detailed agreement with data by using the phenomenological model by Désert *et al.* (1990). In particular, we show that the data cannot be explained by postulating weaker UV heating in the disk of M31. We also show that the VSG-deficient model predicts correctly the correspondence between the IRAS colors and the $100\mu m$ emissivity per H atom in the outer disk of M 31.

"Very Small Grains" are a leading candidate for the carrier of the 21 75Å bump in the extinction curve. Our suggested VSG deficiency in M31 is thus consistent with recent HST observations which show evidence for a weaker and narrower 21 75Å bump on the M31 extinction curve. Some speculation is offered as to possible links between Very Small Grains and the low rate of current star formation in M31.

Subject headings: galaxies: individual - galaxies: interstellar matter - galaxies: photometry - interstellar: grains

1. Introduction

It is now widely accepted that small grains ($\lesssim 100$Å) are an important ingredient of interstellar dust (Puget & Léger 1989). Accurate determinations of the ultraviolet (UV) extinction curve towards a variety of stars using the International Ultraviolet Explorer (see Mathis 1990 for a review) revealed that the extinct.io]l cross section of dust keeps rising from the optical towards the UV, with a 'bump' near 21 75Å, and a non-linear rise in the far UV ($\lambda \gtrsim 2000$Å). This behavior cannot be attributed to large grains ($\gtrsim 100$Å) which, because of their large size, contribute mainly to the near-il]frarccl and optical extinction (Draine & Lee 1984). Near infrared and mid-infrared spectroscopic studies of a wide variety of objects (HII regions, reflection nebulae, planetary nebulae, interstellar cirrus, galaxies) revealed a set of emission features at 3.3, 6.2, '7.'7, 8.6, and 11.3 μm, which have been successfully associated with 1 'olycyclic Aromatic Hydrocarbon molecules (} 'All) by Léger & Puget (1 984, see also Puget & Léger 1989). These are 2-dimensional molecules of $\sim$ 1011 in size, which arc heated by a single photon to more than 1000 K and then reemit the energy mostly in the "aromatic" infrared features. Empirical arguments (Helou, Ryter & Soifer I 991) and model calculations have suggested that they dominate the 12μm IRAS flux of various objects including galaxies (XU & De Zotti 1989).

These PAHs however have difficulty accounting for the diffuse 25μm radiation seen in the Solar Neighborhood (Boulanger & Pérault 1989), in the Galactic plane (Cox & Mezger 1988; Pérault *et* al. 1 988), ant] in nearby galaxies such as M31 (Walterbos & Schwering 1987), without getting uncomfortably large (well over 1000 carbon atoms), and losing their }'All character (Désert *et al.* 1990, hereafter DBP90). Large grains in thermal equilibrium on the other hand cannot account for the diffuse 25μm emission because they arc too cool ($\sim$ 201{, Draine & Anderson 1985). Désert *et al.* (1990) therefore suggested a population of 3-dimentional very small grains (VSG) of size 10-150Å as the predominant source for the diffuse 25μm radiation. Similar to PAHs, VSG undergo significant temperature fluctuations when heated by optical or UV radiation, but reemit the energy in the mid-infrared continuum rather than in features. These VSG will in addition contribute to the 60μm diffuse radiation, a desirable feature in view of the constant 60μm to 100 μm flux ratio in the Galactic plane (Cox & Mezger 1987, Pérault *et al. 1990)* and in the disk of M31 (Walterbos & Schwering 1987). This constancy is reproduced by the combination of VSG and large grains, but is quite

unlikely behavior for large grains alone whose temperatures must decrease substantially from inner to outer disk with the decrease of the radiation field (Helou 1989).

While the properties of PAH molecules are well studied both astronomically and in the laboratory, very few studies in the literature are devoted to VSG, and these studies are exclusively confined to Galactic objects (Sellgren 1984; Castelaz, Sellgren & Werner 1987; Draine & Anderson; DBP90). This is basically due to the difficulty of spectroscopic measurements beyond 20/1111, where VSG emit most of their radiation. For galaxies outside the Milky Way, there is the additional obstacle that the total fluxes at $25\mu m$ and at $60\mu m$ are very often dominated by the warm dust associated with star-formation regions (XU & De Zotti 1989; Rice et al. 1990), so that information about the VSG in the diffuse medium is effectively masked. Consequently, little is known about the nature of VSG. The small graphite grain hypothesis has been favored by many authors because these same grains are strong candidates for providing the 2175Å bump in the UV extinction curve (Draine 1990, Mathis 1990). It is completely unclear however where and how VSG form, and what determines the abundance of VSG relative to "classical" large grains. Helou, Ryter & Soifer (1991) have shown that the abundance of PAHs relative to large grains is constant with a rms dispersion of about 40% among galaxies; however, the question of VSG abundance variations from galaxy to galaxy has not been addressed.

We report here on a study of the IRAS colors of small areas a few hundred pc in size within the disk of M31 . This galaxy is perhaps the best target for studying VSG outside the Milky Way using IRAS data, because: 1) it is the nearest spiral galaxy outside the Milky Way, thus it is well resolved by IRAS; 2) it is a well known quiescent galaxy (Walterbos 1987), and therefore at $60\mu m$ and even at $25\mu m$ the emission is still dominated by the diffuse dust *not* associated with the star-formation regions. The study uses new high resolution ($\sim 1'$) IRAS maps. We find the IRAS color-color diagram of the diffuse emission of M31 to be unusual compared to Galactic cirrus, showing a trend of having rather low $60\mu m$-to-$100\mu m$ surface brightness ratios and high $12\mu m$-to-$25\mu m$ ratios. This observation can be most naturally explained by a deficiency of VSG in M31 . Throughout this paper, we assume for M31 a distance of 690 kpc ($1' = 200$ pc along the major axis), an inclination angle of 77°, and P.A. = 37°.

2. The Data

The new high resolution IRAS maps at 12, 25, 60 and 100μm were obtained from the high resolution processor (HiRes) developed at the Infrared Processing and Analysis Center (IPAC) and based on the Maximum Correlation Method described by Aumann, Fowler & Melnyk (1990). The resolution achieved in these maps is $\sim$ 0.5' x 0.9' (in-scan and cross-scan half-power diameters respectively) for the 12 and 25μm maps, $\sim$ 0.8' x 1' for the 60μm map, and $\sim$ 1.5' x 1.5' for the 100μm map. However, the resolution is not uniform over the maps (Fowler & Aumman 1993), and depends in particular on the surface brightness of the background. In order to overcome this problem, and also to simplify the comparison between the four maps, we smooth all of them to a 1.7' circular beam on a grid with 0.5' pixels. Furthermore, the quantitative analysis in this paper is carried out on a sample of small areas ('cells'), rather than pixels, each of size 2' x 2'. The surface brightness at wavelength λ (λ : 12, 25, 60, and 100 pm), I_λ in Jy sr^{-1}, of each cell is calculated from the corresponding smoothed map by averaging the surface brightness of a 4x4 array of adjacent pixels. These precautions should have essentially removed the problem of ununiform resolutions of the HiRes maps (Fowler, private communication).

Several versions of reduced IRAS data on M 31 have been published, reporting a variety of values for its total integrated fluxes, as shown in Table 1. While we are more concerned With the surface brightness distribution than with the total flux, this is the simplest way to compare the various data sets. The first three sets of numbers are reproduced from the listed references, while the fourth set was measured from the IRAS Sky Survey Atlas (ISSA; Wheelock et al. 1994) using the same method that we, used to extract total fluxes from the HiRes maps. The method consisted of estimating the local background sky brightness in about twenty circular areas of 10 arcminute radius, verifying that these estimates were consistent with a constant background, removing the latter, then spatially integrating the emission from the galaxy. The sources of the uncertainty of M31 integrated fluxes calculated in this work are discussed in Appendix.

There is substantial discrepancy between the various determinations of the M31 fluxes, reflecting primarily improvements in data processing techniques, and small revisions to the calibration of IRAS data. Our HiRes data show very good agreement with ISSA at 60 and 100μm, but run larger than ISSA by about 25% at 12 and 25μm, signalling a possible calibration error. Although the astronomical result we report in this paper is based mainly on the deficiency of 60 μm emission related to 100/111 emission, which is not affected by the discrepancy found here, it also involves, to some extent, the excess surface brightness at 25μm relative to 60 μm, which has the same sign as the

TABLE 1.

Reference	$f_\nu(12\mu m)$	$f_\nu(25\mu m)$	$f_\nu(60\mu m)$	$f_\nu(100\mu m)$
Walterbos & Schwering 1 *987*	175 ± 10	150 ± 5	610 ± 5	2850 ± 100
Rice et al. 1988	163	108	536	2928
Rice et al. 1993	135	99	496	2507
ISSA 1993	172	146	619	3223
This work 1994	217 ± 52	183 ± 38	615 ± 29	3089:1 309

discrepancy of HiRes fluxes compared to ISSA fluxes. However, the magnitude of this discrepancy is too small to affect our main conclusions significantly.

3. IRAS color-color diagrams

With the four IRAS bands one can construct maximally three *independent flux* ratios ('colors'), for which we choose $R(12, 25) = I_{12\mu}/I_{25\mu}$, $R(25, 60) = I_{25\mu}/I_{60\mu}$, and $R(60, 100) = I_{60\mu}/I_{100\mu}$. IRAS color-color diagrams are powerful tools for studying both the grain composition (PAH, VSG, silicate, graphite, etc..) and the heating process of dust in different environment (e.g. in star-formation regions or in quiescent interstellar space). Helou (1986) suggested a two-component model which interprets the anticorrelation between $R(60, 100)$ and $R(12, 25)$ of *galaxies* as resulting from the superposition of two components of FIR emission from interstellar dust: a warm component with high $R(60, 100)$ and low $R(12, 25)$, and a cool component with low $R(60, 100)$ and high $R(12, 25)$. The warm component is in general associated to massive star formation regions, while the cool component is associated with "cirrus" or with quiescent molecular clouds heated by the interstellar radiation field (ISRF). Xu & De Zotti (1989) associated this model with a more realistic grain model which includes PAH, and applied it to the $R(60,100)$ *vs* $R(12, 25)$ diagrams and $R(60, 100)$ *vs* $R(25,60)$ diagrams of both star-forming galaxies (Markarian galaxies) and normal spiral galaxies. Sauvage, Thuan & Vigroux (1990) showed, in the case of the Magellanic Clouds, that the two-component model also applies to regions within galactic disks.

We study the IRAS color-color diagrams of a complete sample of small cells in M31. Each cell, 2' x 2' in size, corresponds to a small region of 0.4 *kpc* x 1.8 *kpc* in the M31 disk. We have included only those cells which are within 80' from the center in

the plane of M31 ($r \leq 16$ kpc for the assumed distance of 690 kpc). We only consider cells with surface brightness sufficiently high that each of the IRAS color ratios plotted in the following figures is significant at least at the 3σ level.

In Figure 1 plotted is the color-color diagram $R(60, 100)$ *vs* $R(12, 25)$ for the M31 cells. The plus signs show the colors of the bulge region, a central elliptical area of $20' \times 12'$ (Walterbos & Kennicutt 1988), which is warmer in emission compared to the disk in both $R(60, 100)$ and $R(12, 25)$. Soifer *et al.* (1987) have found that the 12 and $25\mu m$ emission of the M31 bulge includes a substantial contribution from circumstellar envelopes around evolved low mass stars, which is perhaps never significant in galactic disks. On the other hand the 60 and $100\mu m$ fluxes of the bulge are likely due to interstellar dust heated by the intense ISRF supplied primarily by old stars.

The other points in Figure 1 show the disk colors, with various symbols indicating different significance of the contribution from the dust associated with star-formation regions (the warm component), which is estimated from the ratio

$$R_s = f_\nu^s(60\mu m)/f_\nu(60\mu m) , \qquad (1)$$

where $f_\nu^s(60\mu m)$ is the $60\mu m$ flux due to the discrete sources in a cell in clue.sticm, and $f_\nu(60\mu m)$ its total $60\mu m$ flux. The sources, which are exclusively related to giant HII regions or HII region complexes (Rice et al. 1990; Xu et al. 1992), are extracted from the $60\mu m$ map using Gaussian fittings. It is argued that the radiation from these sources represents well the warm component (XU & Helou 1993). As explained in the legend, the solid squares represent the regions where the warm component dominates ($R_s > 0.5$), the crosses the regions where the warm component diminishing ($R_s < 0.2$), and the open squares the cells in the intermediate situation.

The clashed-dotted line is the IRAS color sequence of the California Nebula measured by Boulanger *et al.* (1988), stretching from the most intensely heated region (the left-uppm corner of Figure 1) to the cooler outer parts of the nebula. The distribution of galaxies on the same color-color diagram generally follows this sequence (Boulanger *et al.* 1988; Helou 1989). The clash ed vertical line shows the colors calculated by DBP90 for Galactic cirrus using the three-population dust model with PAHs, VSG, and large grains. The color variation along the line reflects a range in the intensity of the heating radiation from 0.05 to 10 times the ISRF in the Solar Neighborhood. The line is vertical because in the DBP90 model the spectral shapes of PAH and VSG emission and their relative intensity are almost independent of the intensity of heating radiation.

~'here is a clear trend in this diagram that cells with larger R_s ratios show warmer $R(60, 100)$ *and* cooler $R(1\,2, 25)$ ratios. This is in good agreement with the two-component model (Helou 1986). It should be pointed out that the data points in the bulge do not follow the two-component model, simply because the mechanism of the M 1 R–F] R emission there is somewhat different. However, it contributes so little ($\sim$10%) to the integrated emission of M31 that the validity of the two-component model for the global colors of normal spiral galaxies is not affected.

On the other hand, most of the emission in the M31 disk, especially that from the cells with little contribution from the sources (the crosses), has cooler $R(60, 100)$ and warmer $R(1\,2, 25)$ ratios than the cirrus in the Solar Neighborhood ($R(60,100) = 0.21 \pm 0.01$ and $R(12, 25) = 0.764\ 0.30$, Boulanger & Pérault 1988). This cannot be duc to the difference in the intensity of ISRF because the entire trajectory of the cirrus model (the dashed line) which spans a very wide range of 1S}0' intensity (0.05 - 10 times of the local ISFR), lies near the upper-left border of the data domain.

The problem is presented even better in the $R(60, 100)$ *vs* $R(25, 60)$ diagram which is plotted in Figure 2. Cells in the bulge have been excluded to simplify the plot. The points are coded by the ratio R_s as in Figure 1. The dashed-axlcl-clotted curve again represents the color sequence of the California Nabula. The dashed line is the DBP90 model prediction for Galactic cirrus, with lower $R(25, 60)$ corresponding to more intense heating. Cirrus colors as observed in the Solar Neighborhood (Boulanger & Pérault 1988) occur near the minimum of this curve. Clearly, this color-color diagram allows better discrimination at lower heating intensities then Figure 1, with the points separating out in R_s ratio, and spreading out in a weak anticorrelation $R(60, 100)$ *vs* 1{(25,60). The data, especially those for the cells with little contribution from the sources (the crosses), are clearly inconsistent with the model prediction for Galactic cirrus.

4. 1 nterpretation

4.1. Physical argument

The diffuse emission from the disk of M31, represented by the cells of $R_s < 0.2$, displays IRAS colors which are different from Galactic cirrus: The mean IL(60,1OO) of these cells, 0.167:10.003, is significantly lower than the ratio R(60,100) = 0.21:1 0,01 for the cirrus in the Solar Neighborhood (Boulanger & Pérault 1988), and the mean $R(12, 25) = 1.23 \pm 0,03$ is significantly higher than that of the Solar Neighborhood

cirrus. In the R(60,100) vs R(25,60) diagram, many of these cells show high $25\mu m$-to $60\mu m$ surface birghtness ratios (> 0.5) and low $60\mu m$- to-$100\mu m$ surface brightness ratios (< 0.2) at the same time. The mean R(25,100) = 0.047 ± 0.002 of cells With R_s <0.2 is slightly lower than that of the Solar Neighborhood cirrus.

The constant R(60,100) in the diffuse emission in the Milky Way is interpreted as due to the contribution of emission from 'very small grains' (VSG) (Cox & Mezger 1987, Pérault *et al.* 1990), whose contribution determines the minimum It(GO,] 00) reached at low radiation densities. The unusually low R(60,100) values in the diffuse medium of M31 must therefore indicate a deficiency in VSG emission. This might reflect either a lack of UV heating (Milliard 1984) that drives VSG fluctuations, or a lack of VSG.

A weak UV radiation field would depress even more noticeably the $12\mu m$ emission, because the latter is clue primarily to PAHs which arc more efficient than VSG at absorbing far UV photons. Since the $12\mu m$ emission is *not* depressed (relative to $100\mu m$) in the M31 regions in question, a weak UV field is an unlikely hypothesis.

On the other **hand**, VSG can be heated to relatively high temperatures (~ a few hundreds Kelvin, Draine & Anderson 1985) by a single UV or optics] photon. They are therefore likely to be the most important contributors to the diffuse (cirrus) $25\mu m$ emission as w c]] as the $60\mu m$ emission in regions of low radiation density. It would therefore seem that the more natural explanation of the IRA S colors of M31 cirrus is a deficiency in VSG compared to normal large grains and PAHs.

It should be noted, however, that the integrated IRAS colors of M31 , calculated from the fluxes in 'J'able. 1, do not indicate compellingly a VSG-deficient I S M , probably bemuse the evidence is masked by the superposed emissions from various dust populations (e.g. the diffuse dust in the disk and the dust associated to the star-formation regions) at different heating intensities.

In what follows, wc will use the phenomenological dust model of Désert *et al.* (1990) to clarify and illustrate the above arguments and verify the detailed agreement between the data and our conjecture.

4.2. Model Comparison

In Figures I ant] 2, the dotted line shows the prediction by the DBP'90 model, when dust is heated by a Solar Neighborhood ISRF with the UV light removed, scaled in intensity by a factor varying from 0.05 to 10. This lJV-free model fails to reproduce the data, primarily because it predicts too low a 1/(12, 25) ratio in Figure 1, as might be expected since the UV photons would have provided the greater temperature flue.tuatio]ls (in both VSG and l'A]]), and the associated warmer mid-infrared emission.

In Figure 2, the UV-free model predicts too low a value of $R(25, 60)$, because both PAH and VSG emissivity drops, affecting the flux at $25\mu m$ slightly more than the flux at 60 μm, which still gets contribution from the large grains.

The solid lines in Figures 1 and **2** show the prediction by the D BP90 model modified by reducing the VSG abundance to half its value in Galactic cirrus, This variation on the model provides the best fit to the data. $R(60,100)$ is reduced because of a smaller contribution from VSG to $I_{60\mu}$, whereas R(12, 25) is enhanced because of the increased abundance of PAHs relative to VSG, in agreement with the data in Figure 1. As the intensity of the heating radiation drops below the Solar Neighborhood value, large grains cool down, so their reduced contribution at $60\mu m$ causes the increased $R(25, 60)$ values, thus aligning model predictions and data in Figure 2. At the lowest heating levels the large grains are so cold that their emissivity at $100\mu m$ drops enough to cause the up-turn in the solid line on Figure 2.

in Figure 3 we extend the testing of the VSG-deficient model by examining the emissivity per HI atom. We plot $R(60,100)$ *vs* IR (25, 60) for cells outside the well known bright ring (7 kpc $\lesssim$ r $\lesssim$ 12 kpc), i.e. cells in the annulus 12 kpc $\lesssim$ r $\lesssim$ 14.5 kpc; outside of 14.5 kpc the signal-to-noise ratio drops below 3 everywhere. This annulus offers a reasonably broad range of heating intensities, but remains sufficiently narrow to avoid potential effects due to radial gradients in metallicity and dust-to-gas ratios (Walterbos & Kennicutt 1988). The conditions for dust emission in star-formation regions are very different from those for diffuse dust emission, thus we exclude the cells with $R_s > 0.5$ in order to concentrate on the diffuse dust emission. The points in Figure 3 are marked according to $E(100, HI) = I_{100\mu}/N_{HI}$ ratio in units of $MJy\,sr^{-1}10^{20}H$ cm^{-2}; solid squares are cells with E(100, HI) > 0.4, open squares are cells with 0.2 $\lesssim$ E(100, HI) $\lesssim$ 0.4; and crosses the cells with E(100, HI) <0.2. The cirrus in the Solar Neighborhood has $E(100, HI) = 0.854 \pm 0.03$ in the same units (Boulanger & Pérault 1988). Other symbols have the same meanings as in Figure 2. The three numbers (0.15, 0.85, 3) along the solid line give the values of E (100, HI), as predicted by the model at the corresponding positions on that line, assuming a Solar Neighborhood dust- to-gas ratio (DBP90). 'There are also corresponding tick marks on the dotted line (the cirrus model) and the dashed line (the UV-free model).

The VSG-deficient model (the solid line in Figure 3) fits the data much better than the other two models, namely standard and UV-free Galactic cirrus. In the diagram, the low E(100, HI) points (open squares and crosses), and the high E(100, HI) points (solid squares) are well separated as anticipated from the model. However, the boundary between the two sets of points occurs where the model predicts E(100, HI) $\sim$ 0.85 rather

than $\sim$ 0.4 as required by the measurements. This is likely due to a dust-to-gas ratio which is depressed in the outer disk of M31 compared to the Solar Neighborhood which was used as the basis of the DBP'90 model (Walterbos & Kennicutt 1988). A dust heating model (Xu & Helou 1993), which makes use of available UV, optical and HI maps, and which fits well the spatial distribution of FIR surface brightness in M31, confirms that the dust-to-HI-gas ratio at a galactocentric distance of $\sim$ 14 kpc is about a factor of 2 lower than the Solar Neighborhood value, just as required by the data.

We therefore conclude that the data are compatible with the model predictions of DBP'90 assuming that the VSG abundance relative to large grains and PAHs in M31 is only one half of its value in the local Milky Way.

5. Discussion

We find a significant difference in the IRAS colors of the diffuse dust emission of M31 compared to the large-scale emission (cosecant law) in the Solar Neighborhood. The difference cannot be reproduced by the DBP'90 model assuming UV-deficient heating of the dust in M31. It can be explained however by the same model assuming a VSG abundance half of that in the Solar Neighborhood. This assumption also predicts the locations in the IRAS color-color diagrams of cells in the outer regions of the M31 disk with low and high $I_{100\mu}/N_{HI}$ values. While the modelling works consistently for all M31 cells, the effect is most obvious where the radiation field is the weakest.

The VSG deficiency in M31 would remain a model-dependent result if based solely on the IRAS data, since no direct VSG signature is involved, and DBP'90 may have oversimplified PAH and VSG properties, especially at low heating levels. One hint to this effect is that the model tends to predict an overabundance of VSG at high radiation densities, as evident in Figures 10 and 11 of DBP'90. However, a strong independent argument in favor of the VSG deficiency would be provided by a weaker 21 75Å bump, in line with the suggestion (Mathis 1990) that VSG are responsible for that bump. Recent HST data do indeed reveal narrower and weaker 21 75Å bumps in the extinction spectra derived for two stars at opposite sides of M 31 located about 8 and 11 kpc from the nucleus (Hutchings *et al.* 1992). We therefore conclude that there is significant evidence for a deficiency of VSG in M31 comparing to the Galaxy.

While the VSG abundance in the Solar Neighborhood appears to be typical for the Milky Way (DBP'90, Boulanger & Pérault 1988), the occurence of VSG-deficient regions in our Galaxy cannot be ruled out, especially at low illumination levels or

outside the Solar circle. Such occurences would be similar to the strong variations in I'All abundance reported for pockets within molecular cloud complexes (Boulanger *et al.* 1 990). On the other hand, the integrated colors of even the coldest galaxies remain higher in $R(60,1\ 00)$ than all the model curves in Figure 3 (Helou *et al.* 1 993), suggesting that as in M31, the mixing of emission from different heating environments masks the evidence. No statement can therefore be made about the fraction of galaxies with VSG deficiency as observed in M31, or about the relation between VSG and PAH abundances.

In view of this uncertainty, we can only speculate as to the causes of VSG deficiency, and its implications for the origin of VSG. If the deficiency is tied to the quiescence of M31 in terms of recent star formation (Walterbos 1987), it might indicate that VSG are not formed like large grains, and possiblly the PAH molecules too (Mathis 1990), in the atmospheres of AGB stars, but rather require dense molecular clouds or supernova explosions as their birth places. Alternatively, VSG may require constant processing by supernova. shock waves an cl/or strong UV radiation to avoid growing mantles and turning into large grains.

Acknowledgements. We arc very grateful to Dr. E. Brinks for providing the 111 map of M31 , to Dr B. Milliard for the UV (2000Å) map, and to Dr. R. Walterbos for the optical photometry maps. Helpful discussions with C. Beichman and J. Fowler arc acknowledged. A large part of the work was done when CX held an Alexander von Humboldt Fellowship. This research is supported in part through the IRAS Extended Mission Program by the Jet Propulsion Laboratory, California Institute of Technology, under a contract with the National Aeronautics and Space Administration.

Appendix. Sources of uncertainty of M 31 integrated fluxes

In estimating uncertainties on the final M31 fluxes from this work (Table 1), we consider four sources of uncertainty:

1) Noise in the map: This is estimated from the dispersion in sky brightness away from sources, σ_0, and sets the minimum photometric uncertainty in the surface brightness measured in a pixel, and in the spatially integrated flux in an aperture. The dispersions

measured on the raw HiRes maps within 10′ diameter apertures were 0.29, 0.27, 0.19, and 0.37 MJy/sr at 12, 25, 60 and 100 μm respectively.

Spatial integrals suffer from a minimum uncertainty equal to $N_b^{\frac{1}{2}}\sigma_0$, where N_b is the number of independent resolution elements in the area over which the integration is taken.

2) Background subtraction: The relevant term here is departure from the assumption of a flat background due to structure in the foreground (Milky Way). We have tested for such departures by comparing the statistics of sky brightness in the eighteen 10′ diameter apertures used for background estimation. Each of these areas contains N_b = 1232, 778, 279 or 56 independent resolution elements at 12, 25, 60 and 100μm. The dispersion in the mean surface brightnesses of each area is larger than expected from $\sigma_0 N_b^{-\frac{1}{2}}$, the value expected if σ_0 was the only source of deviation from a flat background. We therefore derive a sky noise component with dispersion σ_1 = 0.02, 0.015, 0.07 and 0.2 MJy/sr on the scale of the test apertures. This will contribute $\sigma_1 N_c^{-\frac{1}{2}}$ to the integrated flux uncertainty, where N_c is the number of 10′ diameter apertures in the solid angle over which the flux is integrated.

The sky noise component characterized only by σ_1 always contributes less than the component due to σ_0 to the uncertainty on the total flux integral of M31. The *combined* terms amount to 45, 35, 15 and 13 Jy at 12, 25, 60 and 100μm; these are in principle the only terms relevant to the comparison between HiRes and ISSA integrated fluxes. Formally, the larger discrepancy at 12 and 25 μm is easily acceptable, since greater uncertainties are expected. The discrepancy at 100μm is probably due to the fact that sky structure (Milky Way cirrus) is more complex than the normal distribution representation adopted here.

3) Calibration:

3.A) The absolute calibration of IRAS data is thought to be uncertain by 10% or less (IRAS Explanatory Supplement 1988). However, this is largely irrelevant to the results in this paper, because the discussion is confined to a comparison of IRAS colors. Moreover, the 11111'90 model has been tied to the IRAS absolute calibration.

3.B) Local deviations of the calibration from the global IRAS calibration are small, typically $\leq$ 5% (ISSA Explanatory Supplement 1994).

3.C) Calibration uncertainties associated with the variation of responsivity of IRAS detectors with "dwell time", or equivalently with source size arise because the HiRes

maps wc work with here usc the very-large-scmrcc responsivity limit, whereas the M31 maps contain structure 011 various scales. The uncertainties should be bo unded by the AC/DC responsivity ratio described in the IRAS Explanatory Supplement (1 988, chapter IV), This ratio amounts to 0.78, 0.82 and 0.92 at 12, 25 and 60μm, but was set to 1 at 100pnl because of the more complex behavior at this wavelength. ¿From Figure IV.A ,4.2 of the IRAS Explanatory Supplement, wc estimate 20% as a reasonable upper limit to this source of uncertainty at 100μm. We have adopted 1 1%, 9%, 4%, and IO% for the uncertainty at 12, 25, GO and 100~~ln.

4) HiRes artifacts: Potential artifacts of HiRes for extended, low surface brightness sources have not been characterized. Point source photometry at relatively high signal - to-noise ratios is expected to be better than 20%. The uncertainties which appear in Table 1 do not include any term for such artifacts.

The contributions from items 1), 2), and 3.C) above arc added in quadrature to yield the uncertainties listed in Table 1,

REFERENCES

Aumann, }1. H., Fowler, J. W. & Melnyk, M., 1990, *Astron. J.* **99**, 1674

Boulanger, F., and Pérault, M., 1988, *Astrophys. J.* 330, 964

Boulanger, F., Beichman, C., Désert, F. X., Helou, G., Pérault, M., and Ryter, C. 1988, *Astrophys. J.* 332, 328

Boulanger, 1'., Falgarone, E., Puget, J.-l,. and Helou, G. 1990, *Astrophys. J.* 364, 136

Castelaz, H.W., Sellgren, K., and Werner, M. W., 1987, *Astrophys. J.* **313**, 853

Cox, 1'. and Mezger, P, 1988, in *Comets to Cosmology*, ed. A. Lawrence, Lecture Notes in Physics 297, Springle, Heidelberg, p.97

Désert, 11'. A., Boulanger, F., and Puget, J.L., 1990, *Astron. Astrophys.* 273, 215 (DBP90)

Draine, B.T., and Anderson, N., 1985, *Astrophys. J.* 292, 494

Draine, B.T., and Lee, H.M., 1984, *Astrophys. J.* **285**, 89

Fowler, J. W., and Aumann, 11. 11., 1993, to appare in proceedings of *Workshop on Science with High Spatial Resolution Far-infrared Data*, (14-16 J une 1 993, IPAC, Pasadena), eds. S. Terebey and J . Mazzarella

Helou, G., 1986, *Astrophys. J.* **311**, 1.33

Helou, G., 1989, in *Interstellar Dust*, Proceedings of IAU Symposium 135 held in Santa Clara, CA, 26-30 July 1988, ed. L.J. Allamandola & A.G.G.M. Tielens (Dordrecht: Kluwer), p. 285

Helou, G., Ryter, C. and Soifer, B.T., 1991, *Astrophys. J.* **376**, 505

Helou, G. *et al. 1993,* in preparation

Hutchings, J .B. *et al.* 1992, *A strophys. J. 400,* 1,35

Léger, A., and Puget, J.],., 1984, *Astron. Astrophys.* **137**, 1.5

Mathis, J. S., 1990, *Ann. Rev. Astron. Astrophys. 28, 37*

Milliard, 11., 1984, *Thesis,* Université de Provence Aix - Marseille 1

Pérault, M., Boulanger, F., Puget, J .L., and Falgarone, E., 1988, unpublished

Puget, J.],., and Léger, A., 1989, *Ann. Rev. Astron. Astrophys. 27,* 161

It.ice, W., Boulanger, F., Viallefond, F., Soifer, B.T., Freedman, W.],., 1990, *A strophys. J. 358, 418*

11.ice, W., Lonsdale, C. J., Soifer, B. 'J'., Neugebauer, G., Kopen, E.L., Lloyd, L. A., de Jong, T., and Habing, H. J., 1988, *Astrophys. J. Suppl.* **68**, *91*

Rice, W., 1993, *Astron. J.* **105**, 67

Savage, B.D., and Mathis, J. S., 1990, *Ann. Rev. Astron. Astrophys. 17,* 7 3

Sauvage, M., Thuan, 'J'. X., and Vigroux, L., 1990, *Astron. Astrophys.* **237**, 296

Sellgren, K., 1984, *Astrophys. J.* 277, 623

Soifer, B.T., Rice, W., Mould, J .R., Gillett, F. C., Rowan-Robinson, M., and Habing, 11., 1986, *Astrophys. J. 304,* 651

Walterbos, It.. A.M., 1987, in *Galactic and Extragalactic Star Formation*, eds. R.E. Pudritz and M. Fich. Kluwer, Dordrecht, p361

Walterbos, R.A.M., and Kennicutt, R., 1988, *Astron. Astrophys.* 198, 61

Walterbos, R.A .M., and Schwering, P.B.W., 1987, *Astron. Astrophys.* **180**, 27

XU, C., and De Zotti, G. 1989, *Astron. Astrophys. 225,* 1 2

Xu, C. and Helou, G. 1993, in preparation

Xu, C., Klein, U., Meinert, D., Wielebinski, R., Haynes, R.F., 1992, *Astron. A strophys.* 257, 47

Figure captions

Figure 1 $R(60,100)$ *vs* 1/(12, 25) diagram for cells (2' x 2') in M31, The plus signs are cells in the bulge region. Other points are cells in the disk: solid squares are ones with significant contribution from sources ($R_s = f_\nu^s(60\mu m)/f_\nu(60\mu m > 0.5)$, open squares with intermediate R_s ratio ($0.2 \leq R_s \leq 0.5$), and the crosses are dominated by the diffuse emission ($R_s < 0.2$). For comparison the corresponding ratios of the cirrus in Solar Neighborhood is given in the upper-right corner of the figure. The dashcel-dotted line is the color sequence of the California Nebula (Boulanger et al. 1988), which goes from the center of the star-forming region (the left-u])per corner of the figure) to the outer part of the nebula. Galaxies are usually located near this line. The clash cel vertical line is the model prediction by Désert et al. (1 990) for the Galactic cirrus. The range of the intensity of ISRF in the model caculation is 0.05 - 10 times that of in the Solar Neighborhood. The clotted line is the prediction of the same dust model but heated by an ISRF without any UV light. The solid line is the prediction from a model which is otherwise the same with that of Désert et al. (1 990), but the abundance of Very Small Grains (VSG) is multiplied by a factor of *0.5*.

Figure 2 $R(60,$ **100)** *vs* $R(25,60)$ diagram for cells (2' x 2') in M31 disk. Cells in the bulge regions (the plus signs in Fig.1) have been deliberately excluded. Other symbols have the same meanings as in Figure 1.

Figure 3 $R(60,$ 100) *vs* $R(25,$ *60)* diagram for cells (2' x 2') in M31 outer disk (12k~Jc $\leq$ r $\leq$ 16 kpc). Only cells with $R_s \leq 0.5$ arc included. They are marked according to the $I_{100\mu}/N_{HI}$ ratio: solid squares are ones with $I_{100\mu}/N_{HI}$ >0.4 (MJy sr^{-1}/ 1 0^{20}11 cm^{-} 2), open squares with $0.2 \leq I_{100\mu}/N_{HI} \leq 0.4$(MJy sr^{-1} /10^{20}11 cm^{-} 2), and crosses with $I_{100\mu}/N_{HI} < 0.2$(MJy sr^{-1}/1 0^{20}11 cm^{-} 2). Other symbols have the same meanings as in Figure 2. '**J)he** three numbers (0.15, 0.85, 3) along the solid line give the $I_{100\mu}/N_{HI}$ values, in units of MJy sr^{-1} /102°11 cm^{-2}, predicted by the model at the corresponding positions on that line assuming a local dust-to gas ratio (Désert et al. 1990). Tick marks on the other two n odel lines correspond to the same $I_{100\mu}/N_{HI}$ **Value%.**

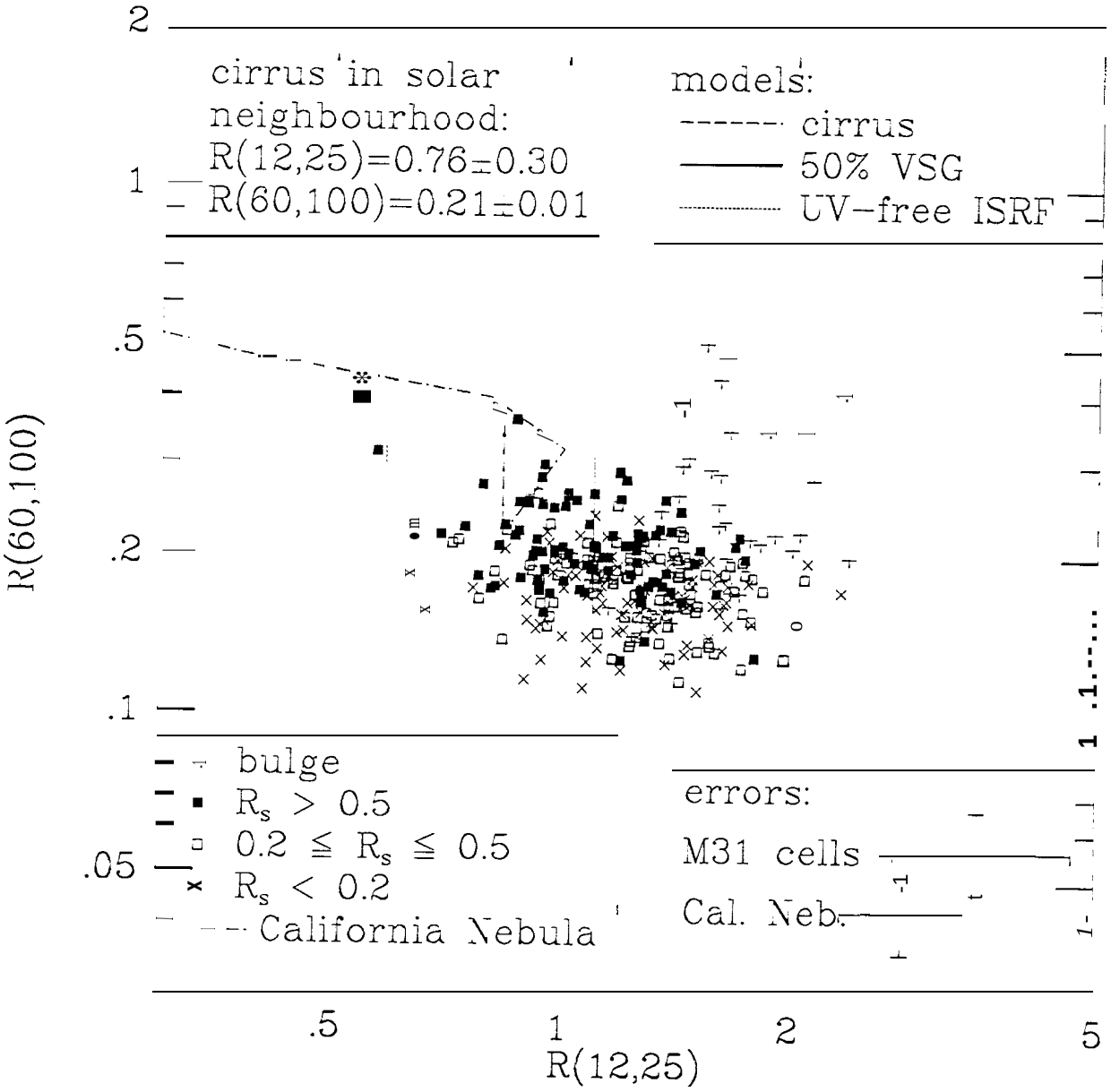
cirrus in solar neighbourhood:
R(12,25)=0.76±0.30
R(60,100)=0.21±0.01
models:
cirrus
50% VSG
UV-free ISRF
bulge
$R_s > 0.5$
$0.2 \leq R_s \leq 0.5$
$R_s < 0.2$
California Nebula
errors:
M31 cells
Cal. Neb.
R(60,100)
R(12,25)
2
1
.5
.2
.1
.05
.5
1
2
5

Figure 1

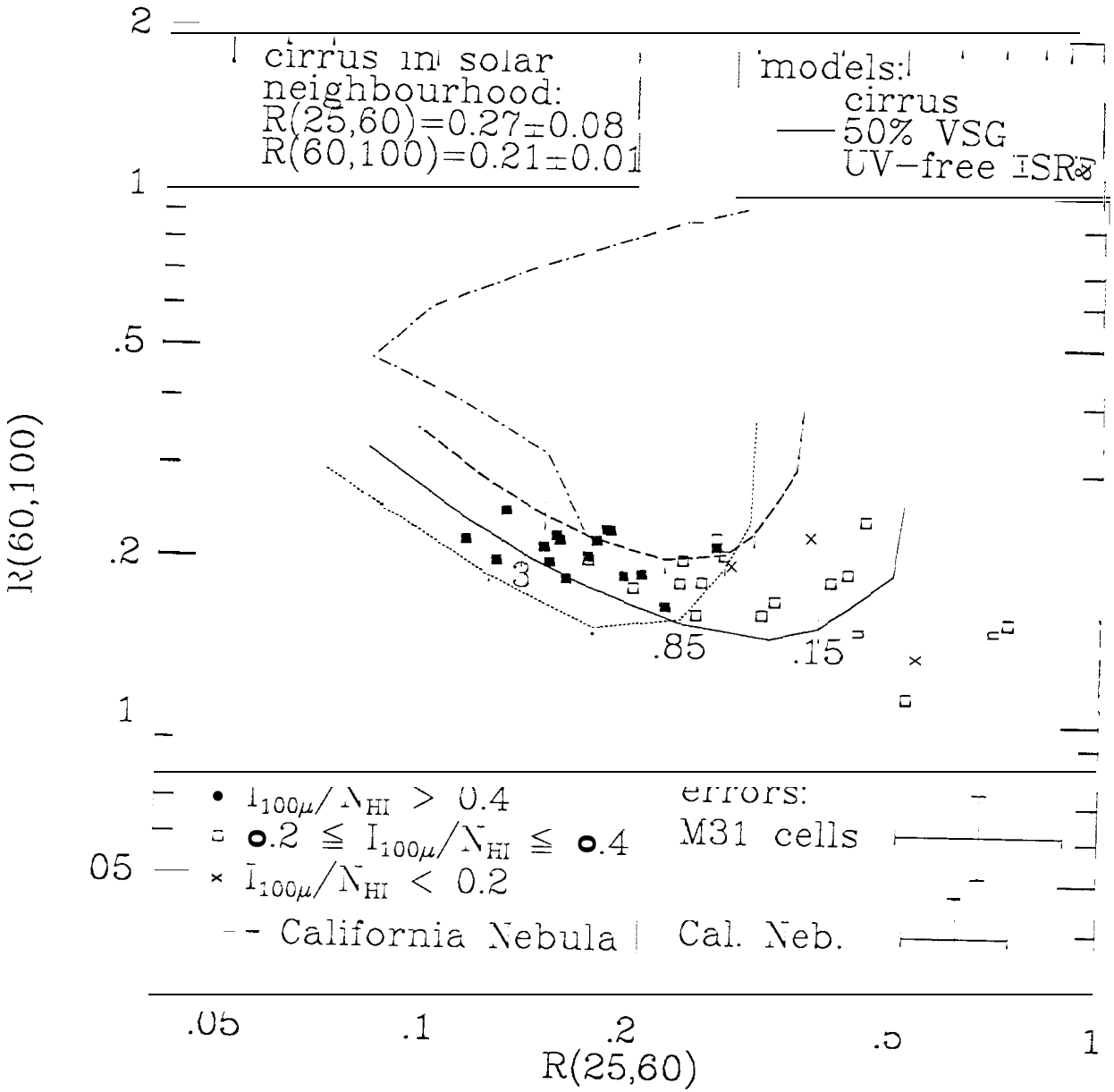
cirrus in solar neighbourhood:
R(25,60)=0.27±0.08
R(60,100)=0.21±0.01
models:
cirrus
50% VSG
UV-free ISRF
.3
.85
.15
• $I_{100\mu}/N_{HI} > 0.4$
o.2 ≦ $I_{100\mu}/N_{HI}$ ≦ o.4
× $I_{100\mu}/N_{HI} < 0.2$
California Nebula
errors:
M31 cells
Cal. Neb.
R(60,100)
R(25,60)
2
1
.5
.2
1
05
.05
.1
.2
.5
1

Figure 2

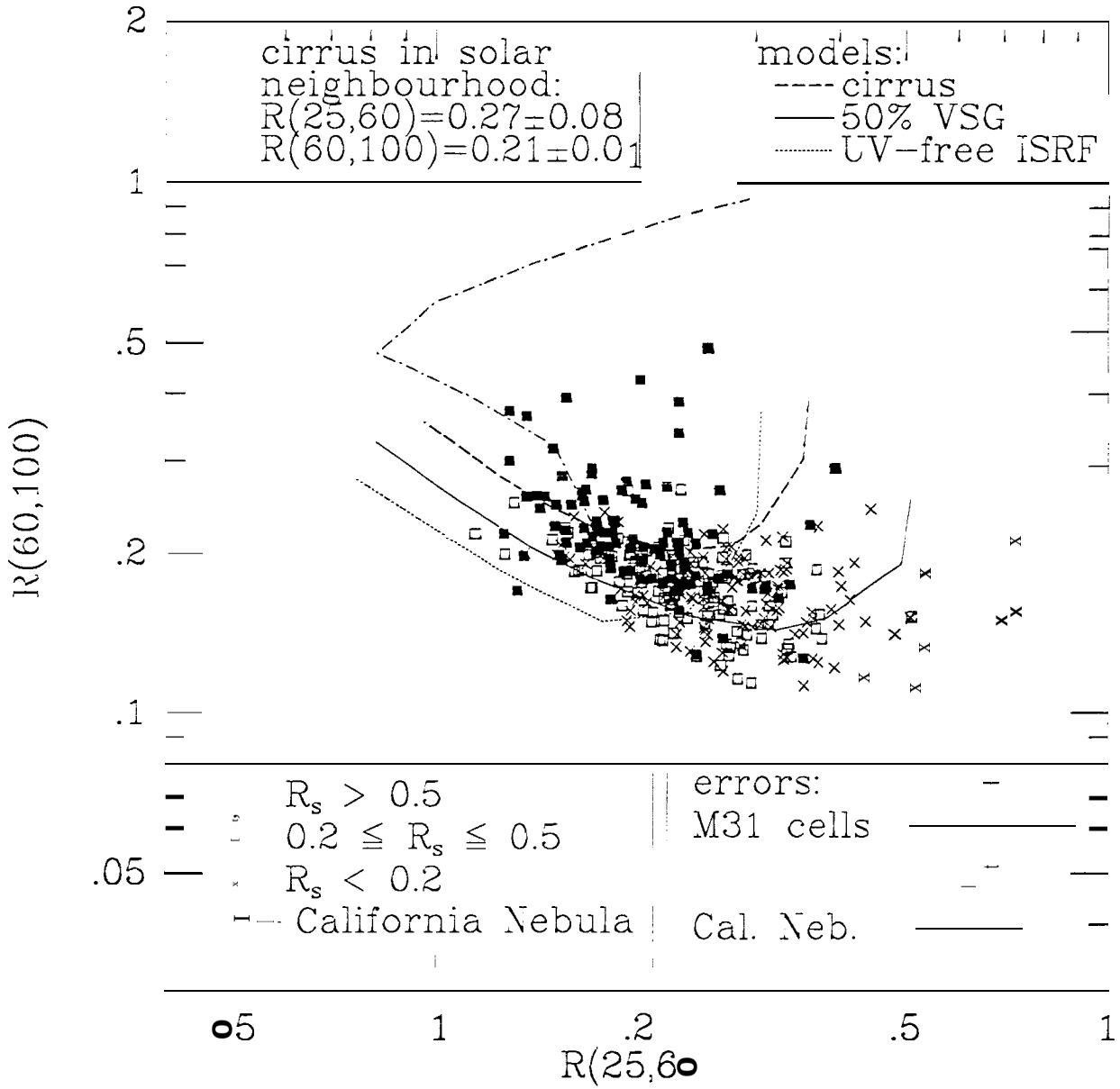
cirrus in solar neighbourhood:
R(25,60)=0.27±0.08
R(60,100)=0.21±0.01
models:
cirrus
50% VSG
UV-free ISRF
R(60,100)
R(25,60)
2
1
.5
.2
.1
.05
.5
1
.2
.5
1
$R_s > 0.5$
$0.2 \leq R_s \leq 0.5$
$R_s < 0.2$
California Nebula
errors:
M31 cells
Cal. Neb.

Figure 3